Available online at www.sciencedirect.com
ScienceDirect
Proceedings of the Combustion Institute 32 (2009) 1747–1754
Proceedings of the Combustion Institute
www.elsevier.com/locate/proci

Premixed turbulent flame front structure investigation by Rayleigh scattering in the thin reaction zone regime

Frank T.C. Yuen, Ömer L. Gülder *

Institute for Aerospace Studies, University of Toronto, 4925 Dufferin Street, Toronto, Ont., Canada M3H 5T6

Abstract

Premixed turbulent flames of methane–air and propane–air stabilized on a bunsen type burner were studied using planar Rayleigh scattering and particle image velocimetry. The fuel–air equivalence ratio range was from lean 0.6 to stoichiometric for methane flames, and from 0.7 to stoichiometric for propane flames. The non-dimensional turbulence rms velocity, u'/S_L, covered a range from 3 to 24, corresponding to conditions of corrugated flamelets and thin reaction zones regimes. Flame front thickness increased slightly with increasing non-dimensional turbulence rms velocity in both methane and propane flames, although the flame thickening was more prominent in propane flames. The probability density function of curvature showed a Gaussian-like distribution at all turbulence intensities in both methane and propane flames, at all sections of the flame.

The value of the term $D\kappa$, the product of molecular diffusivity evaluated at reaction zone conditions and the flame front curvature, has been shown to be smaller than the magnitude of the laminar burning velocity. This finding questions the validity of extending the level set formulation, developed for corrugated flames region, into the thin reaction zone regime by increasing the local flame propagation by adding the term $D\kappa$ to laminar burning velocity.

Keywords: Premixed turbulent combustion; Thin reaction zones; Flame curvature; Flame front thickness

1. Introduction

One of the essential pieces of information required in simulation and modeling of the premixed turbulent flames is a measure of the scalar gradient in the flame front [1]. In most modeling approaches the local scalar gradient is through some form of averaged scalar dissipation rate. The scalar gradient information requirement in flamelet models is handled by assuming that the flame front is a thin passive interface that locally propagates with a laminar burning velocity and a scalar structure of a laminar flame front. At Damköhler numbers much larger than unity, a premixed turbulent flame front is taken as consisting of regions of reactants and products separated by thin laminar flamelets. Since the instantaneous behaviour of these thin layers is the same as those of laminar flames, turbulent burning velocity can be approximated by the product of the flamelets surface area and laminar

* Corresponding author. Fax: +1 416 667 7799.
E-mail address: ogulder@utias.utoronto.ca (Ö.L. Gülder).

1540-7489/$ - see front matter © 2009 The Combustion Institute. Published by Elsevier Inc. All rights reserved.
doi:10.1016/j.proci.2008.08.005

burning velocity corrected for the effect of stretch and flame curvature.

The most recent regime diagram for the premixed turbulent combustion [2] extends the traditional flamelet regime, i.e., wrinkled and corrugated flame regions, further up to $Ka = 100$ from the previous upper limit of $Ka = 1$, where Karlovitz number, Ka, is defined as the ratio of chemical time scale to the Kolmogorov time scale. The region between $Ka = 1$ and $Ka = 100$ is called the "thin reaction zones", and the similar flamelet assumptions are claimed to be still valid [2]. In the theory for the thin reaction zones regime [2] the propagation speed of the instantaneous flame is given by $s_\kappa = D\kappa$, where D is the diffusivity and κ is the local flame curvature. It is argued that this value is much higher than the laminar burning velocity in this regime. The proposal that s_κ should be used instead of the laminar burning velocity in the thin reaction zone regime is based on the two-dimensional DNS data [3]. The proposed level set equation for the thin reaction zone regime is a modification of the G-equation, given as [4]

$$\frac{\partial G}{\partial t} v \cdot \nabla G = s_{L,s} \mid \nabla G \mid - D\kappa \mid \nabla G \mid, \qquad (1)$$

where $s_{L,s} = s_n + s_r$, and s_n and s_r are contributions due to normal diffusion and reaction to the displacement speed of the thin reaction zone. However, $s_{L,s}$ is the same order of magnitude as the laminar burning velocity. Therefore the experimentally observed high turbulent burning velocities are accounted for by the $D\kappa$, in the second term on the right hand side of Eq. (1). It is conjectured that the magnitude of $D\kappa$ will be much greater than the laminar burning velocity so that the modified G-equation would be able to represent premixed turbulent combustion in the thin reaction zone regime [4]. However, there is a growing body of experimental evidence that the approaches based on the flamelet hypothesis may not be always valid over the range of conditions corresponding to the thin reaction zones regime, see for example [5–8]. To assess the validity of Eq. (1), the term $D\kappa$ in the equation can be evaluated from the instantaneous flame front curvatures and related statistics which can be measured by laser-based diagnostics.

The main objectives of the current study are to evaluate the term $D\kappa$ in the modified G-equation in the thin reaction zone regime using the measured flame front structure data, and to investigate the role of curvature in propagation of the flame front. The flame front data were obtained using planar Rayleigh scattering on a bunsen type burner fueled by either premixed methane–air or propane–air. The fuel–air equivalence ratio range was from 0.6 to stoichiometric for methane flames, and from 0.7 to stoichiometric for propane flames. The non-dimensional turbulence rms velocity, u'/S_L, covered a range from 3 to 24. Experimental conditions correspond to conditions of the corrugated flames and thin reaction zones regimes as described in [4]. Particle image velocimetry was used to measure instantaneous velocity field for the experimental conditions studied. In this paper, first we present results related to the structure of the premixed flame fronts in the thin reaction zone regime. Then the term $D\kappa$ was evaluated using experimental flame curvature data and computed diffusivities corresponding to conditions in the reaction zone of flame fronts.

2. Experimental methodology

Premixed turbulent conical flames were produced by an axisymmetric bunsen type burner with an inner nozzle diameter of 11.2 mm. Premixed turbulent propane–air flames with equivalence ratios from 0.7 to 1.0, and methane–air flames with equivalence ratios from 0.6 to 1.0 were stabilized by using an annular pilot flame. A premixed methane–air or propane–air flame is used for low turbulence intensities; at higher turbulence levels an ethylene–air flame was used as the annular pilot. Perforated plates positioned three nozzle diameters upstream of the burner rim controlled the turbulence levels.

Particle image velocimetry was used to measure instantaneous velocity field for the experimental conditions studied. Summary of experimental conditions for all flames studied are tabulated in Table 1. The PIV experiment was conducted separately from the Rayleigh scattering experiments. The system consisted a double-pulsed second harmonic (532 nm) Nd:YAG laser working at an energy level of 50 mJ/pulse and a frequency of 15 Hz; a CCD camera with an array size of 1600 × 1186 pixels and equipped with a 2.8 f-number 60 mm focal length camera objective. This optical setup was used to capture the flow condition above the nozzle exit with a view area of 11.6 mm × 15.7 mm and a resolution of 9.8 μm/pixel. The time separation between the two laser pulses was 10 μs. The submicron oil droplets were generated by a nebulizer as seeding particles. The image scale factor was 1.326; the interrogation region was 32 × 32 pixels; and the pixel pitch was 5.56 μm. The multiplication of these terms gives the actual PIV resolution which is about 0.24 mm. This is the smallest velocity structure that can be resolved which is smaller than the Taylor length scales in Table 1. The length scales were estimated by using the velocity field data from the PIV measurements which yielded u'. The auto-correlation functions of u' were calculated along the length of the image. The integral length scales were found by integrating the auto-correlation functions to where they first crossed zero. The Taylor length scales were

Table 1
Summary of experimental conditions

Flame	Φ	Λ (mm)	λ (mm)	η (mm)	u'/S_L	δ_L° (mm)	Re_Λ	Ka	D (cm^2/s)
M1	1.0	1.62	0.45	0.052	3.24	0.446	97.7	1.06	
M2	0.9	1.62	0.45	0.052	3.66	0.476	97.4	1.35	
M3	0.8	1.62	0.45	0.052	4.65	0.537	97.1	2.19	
M4	0.7	1.62	0.45	0.052	6.43	0.677	96.8	4.20	
M5	0.6	1.62	0.45	0.052	10.80	1.002	96.4	11.85	2.96
M6	1.0	1.64	0.44	0.052	3.30	0.446	100.5	1.09	
M7	0.9	1.64	0.44	0.052	3.73	0.476	100.2	1.39	
M8	0.8	1.64	0.44	0.052	4.73	0.537	99.9	2.24	
M9	0.7	1.64	0.44	0.052	6.55	0.677	99.6	4.30	
M10	0.6	1.64	0.44	0.052	11.00	1.002	99.2	12.14	2.96
M11	1.0	1.79	0.46	0.029	7.25	0.446	241.6	3.38	
M12	0.9	1.79	0.46	0.029	8.18	0.476	240.9	4.31	3.37
M13	0.8	1.79	0.46	0.029	10.39	0.537	240.1	6.97	3.32
M14	0.7	1.79	0.46	0.029	14.38	0.677	239.3	13.37	3.26
M15	0.6	1.79	0.46	0.029	24.13	1.002	238.5	37.71	2.96
P1	1.0	1.61	0.42	0.058	2.67	0.337	84.2	0.78	
P2	0.9	1.61	0.42	0.058	3.03	0.358	83.7	1.00	
P3	0.8	1.61	0.42	0.058	3.71	0.399	83.2	1.51	
P4	0.7	1.61	0.42	0.058	5.14	0.476	82.7	2.91	
P5	1.0	1.53	0.41	0.048	3.41	0.337	101.9	1.15	
P6	0.9	1.53	0.41	0.048	3.87	0.358	101.3	1.48	
P7	0.8	1.53	0.41	0.048	4.74	0.399	100.7	2.23	
P8	0.7	1.53	0.41	0.048	6.56	0.476	100.1	4.31	
P9	1.0	1.75	0.44	0.030	6.68	0.337	228.8	2.95	
P10	0.9	1.75	0.44	0.030	7.57	0.358	227.4	3.80	
P11	0.8	1.75	0.44	0.030	9.28	0.399	226.1	5.72	3.33
P12	0.7	1.75	0.44	0.030	12.86	0.476	224.7	11.03	3.24
P13	0.7	1.83	0.46	0.031	12.49	0.476	228.8	10.31	3.24
P14	0.7	1.37	0.41	0.024	16.22	0.476	221.8	17.67	3.24
P15	0.7	1.77	0.43	0.024	17.50	0.476	309.4	17.42	3.24
P16	0.7	1.54	0.44	0.021	20.26	0.476	311.0	23.27	3.24

In the first column "M" refers to methane flames and "P" to propane flames.
Φ is fuel–air equivalence ratio; Λ, λ, and η are integral, Taylor and Kolmogorov length scales, respectively; u'/S_L is non-dimensional turbulence rms velocity; δ_L° is the unperturbed laminar flame thickness calculated by detailed kinetics [16]; Re_Λ is the Reynolds number based on u' and integral length scale Λ; Ka is the Karlovitz number; and D is the molecular diffusivity calculated at 1800 K.

estimated by constructing an osculating parabola for the auto-correlation function. The distance to which the parabola crosses zero is the Taylor length scale.

Flame front images were captured using planar Rayleigh scattering [9–11]. This setup consisted of a third harmonic (355 nm) Nd:YAG laser working at an energy level of 305 mJ/pulse and a frequency of 10 Hz; a set of beam-shaping optics through which the laser beam passed to produce a laser sheet of 60 mm high and 150 μm thick; an intensified CCD camera with an array size of 1024 × 1280 pixels positioned at 90° to the scattered light, and equipped with a 4.1 f-number 94 mm focal length camera objective. With this setup, a capture area of 57 mm × 46 mm and a resolution of 45 μm/pixel were achieved. The signal to noise ratio for the products is about 14.3, and for the reactants 23.8. This is found by calculating the ratio between the mean and standard deviation for an area of 2500 pixels in the product and reaction regions of the flame. Typical Rayleigh scattering intensity is about 260 counts for reactant pixels and 72 for product pixels. However, with this arrangement of the optical layout, it was necessary to divide the flame into three sections along the flame centerline, and images were captured for three sections separately. Each section of the flame has a height of 44 mm and width of 22 mm. The centers of the sections are 66.5, 96.5, and 121.5 mm above the burner rim; these sections were referred as "low", "middle", and "top" sections of the flame, respectively, in Section 3 of the paper. More than 300 images were captured for each experimental conditions.

Rayleigh scattering images were first processed using a 3 × 3 non-linear sliding average filter to reduce noise in the raw images. The total number density of the molecules is directly proportional to temperature by using the ideal gas law and assuming constant pressure conditions. The raw Rayleigh scattering density images were then converted into temperature field using the following expression [12,13]

$$T_{\text{flame}} = \underbrace{\frac{\left(\sum_i \sigma_i \chi_i\right)_{\text{mix}}}{\left(\sum_i \sigma_i \chi_i\right)_{\text{air}}}}_{k} T_{\text{air}} \underbrace{\frac{(I_{\text{air}} - I_{\text{back}})}{(I_{\text{flame}} - I_{\text{back}})}}_{I}, \quad (2)$$

where T_{flame} is calculated for each pixel in each image, σ_i is the Rayleigh scattering cross section for each molecule i, χ_i is the mole fraction of different species, I_{flame} and I_{air} are the Rayleigh scattering signal intensities of the flame and a calibration image with air at temperature T_{air}. I_{back} is the background signal intensity which consisted of the dark noise of the ICCD camera, the laboratory background light and laser reflections. Due to its parasitic nature in the experimental setup, I_{back} was estimated by setting the flame temperature to that of the adiabatic flame and solving Eq. (2) in the product region of the each flame image. I_{back} for each image was calculated so that the flame temperature in the product region was equivalent to adiabatic flame temperature [14]. The background signal was approximately 26 counts and the variation was less than ±3 counts throughout the flame image. So it is reasonable to use a single background count for the entire image.

The Rayleigh scattering cross sections that have been tabulated in [15] were used. The variation of the different combustion species across flame front was obtained through a 1D laminar flame simulation with the Cantera package which uses the GRI-3.0 mechanism [16]. From these data, the variations of the effective Rayleigh scattering cross sections (k, first fraction on the right hand side of Eq. (2)) with temperature were calculated for methane and propane flames. The peaks of the probability density functions of the intensity ratio (I, last fraction on the right hand side of Eq. (2)) which correspond to the burnt and unburned gases were determined. These peak intensity ratio values were then related to the burnt and unburned gas temperatures. In this way, relationships of k versus I were established for different equivalence ratios and fuels. So for each I value, there was a corresponding k value for calculating the flame temperature at each pixel. An instantaneous Rayleigh scattering temperature image is shown in Fig. 1, and an example of a local temperature profile across the flame front is shown in Fig. 2.

The maximum resolution of the Rayleigh imaging system was found using the contrast transfer function (CTF) which corresponds to 22 line-pairs/mm at CTF of 10%. Thus, the limiting resolution for the Rayleigh scattering measurements would be the laser sheet thickness which is 150 μm.

The Rayleigh scattering images were processed to provide instantaneous temperature gradients, ∇T, at progress variable $c = 0.5$ and 0.3, where $c = (T - T_u)/(T_b - T_u)$. T is the instantaneous temperature, T_b is the burnt gas temperature, set equal to the flame temperature calculated from Eq. (2), and T_u is the unburned gas temperature. Thicknesses were calculated using the following expression:

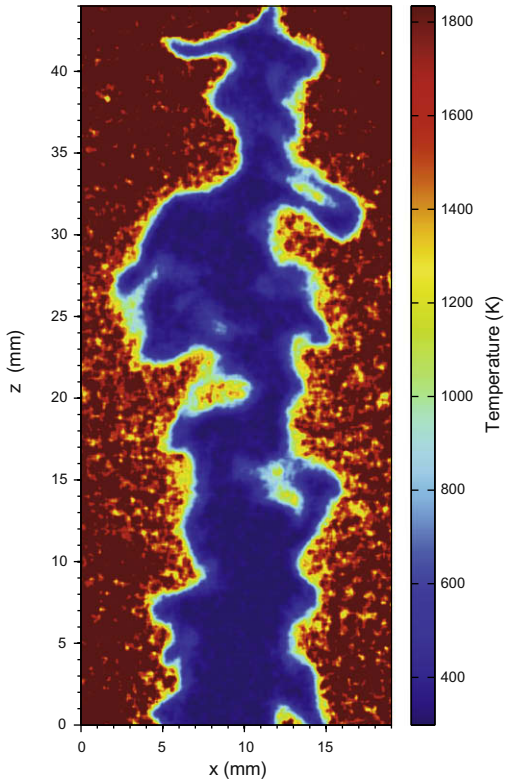

Fig. 1. Instantaneous Rayleigh scattering temperature image for flame condition M9 (Table 1) at an equivalence ratio 0.7 and $u'/S_L = 6.55$.

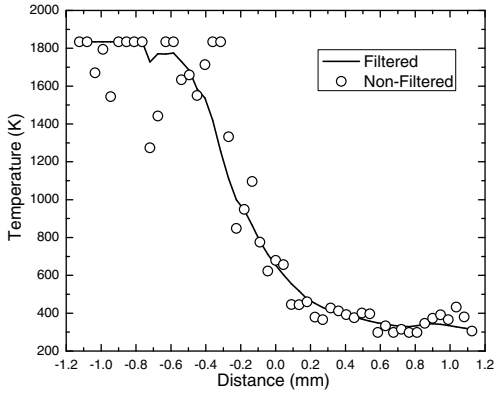

Fig. 2. An example of local temperature profile for the same condition of Fig. 1. Circles are the raw data and line represents 3 × 3 non-linear sliding average filtered data.

$$\delta_{th} = \frac{T_b - T_u}{|\nabla T|_{max}}. \quad (3)$$

The term $|\nabla T|_{max}$ is the maximum temperature gradient along the direction which is normal to the flame front. The flame thickness evaluated at $c = 0.5$ can be considered as the reaction zone thickness, while the one at $c = 0.3$ can be treated as the preheat zone thickness [12,13]. The c contours were found using an edge detection algorithm. Two dimensional ∇T was extracted at each point along those contours. T_u and T_b were found from the probability density function of the temperature distribution of each image. Laminar thermal flame thicknesses (δ_L^0) were calculated from the temperature profiles across a 1D laminar flame simulation. This was performed with the Cantera package which uses the GRI-3.0 mechanism [16].

Using the analysis method described in Wang and Clemens [17], dissipation structures which are larger than laser sheet thickness of 150 μm were found to have a relative error of 9% in flame thickness and 8% relative error for temperature gradients.

After the $c = 0.5$ contour was found, local curvature, κ, at each pixel point along the flame contour was calculated using

$$\kappa = \frac{\dot{x}\ddot{y} - \dot{y}\ddot{x}}{(\dot{x}^2 + \dot{y}^2)^{3/2}}, \quad (4)$$

where $\dot{x} = dx/ds$ and $\ddot{x} = d^2x/ds^2$ are the first and second derivatives with respect to s which is the flame contour length measured from a fixed origin on the flame front [18–20]. After the $c = 0.5$ contours were found, these contours were filtered by a zero-phase digital filter which processed the contours in both forward and reverse direction. These provided no phase distortion and doubled the filter order. The filter length was chosen to be 5-points which provide a filter order of 8. These filtered contours were then differentiated to give their respective first and second derivatives. The derivative curves were filtered again using the same filter and then curvatures were found using Eq. (4). The minimum radius of curvature that can be resolved was found to be limited by the laser sheet thickness which was 0.15 mm. The uncertainty in determining flame front curvature was about 25%. To evaluate the term $D\kappa$, diffusivities are calculated at about 1800 K by using [16] and assuming that the Schmidt number is unity.

It should be noted that the flame front measurements with planar Rayleigh scattering are two-dimensional and there is a concern that planar measurements may not be representative of the three-dimensional flame front structure. However, recently Chen et al. [21] demonstrated that probability density distributions of two and three dimensional flame curvatures are similar although their experiments were done at relatively lower turbulence intensities. This finding suggests that the planar measurements would be sufficient to determine the curvature statistics of the premixed turbulent flames.

3. Results and discussion

Flame front thicknesses evaluated from temperature gradients obtained from two-dimensional Rayleigh scattering measurements show a very mild, if any, sensitivity to non-dimensional turbulence intensity, u'/S_L. The variation of the flame front thickness based on the temperature gradient at progress variable $c = 0.5$ and $c = 0.3$ with methane flames are shown in Figs. 3 and 4, respectively. At all three sections of the flame, the flame front thickness seems to increase slightly with non-dimensional turbulence intensity. Figure 5 shows the same trend in flame front thickness for propane flames at $c = 0.5$, although the increase in flame front thickness with non-dimensional turbulence rms velocity is more pronounced in propane flames than that of methane flames. At $c = 0.3$, the thickness is more related to the thickness of the preheat layer. Figures 5 and 6 indicate that the thickening process with increasing turbulence is more or less the same for both the reaction zone and the preheat zone for propane flames, although the thickness change appears to be more prominent in the reaction zone. In a recent numerical simulation, however, it is found that the thickening process in the reaction zone is much weaker than that in the preheat zone [22].

The probability density functions of methane flame surface curvatures for the middle section of the flames are shown in Fig. 7 at various non-dimensional turbulence intensities. Curvature pdfs display a Gaussian behaviour at all turbulence intensities. Similar trends are also reported in

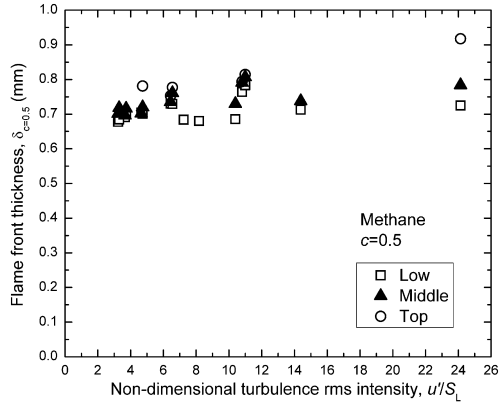

Fig. 3. Flame front thickness at $c = 0.5$ for methane flames as a function of non-dimensional turbulence rms velocity at different sections of the flame.

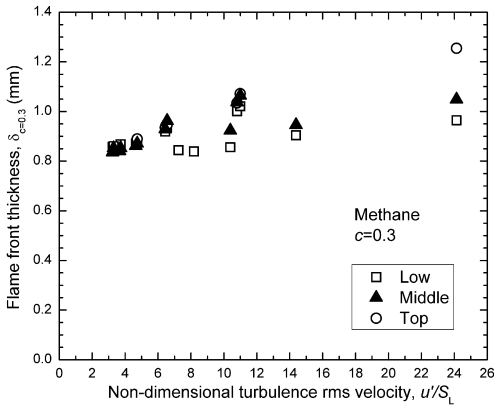

Fig. 4. Flame front thickness at $c = 0.3$ for methane flames as a function of non-dimensional turbulence rms velocity at different sections of the flame.

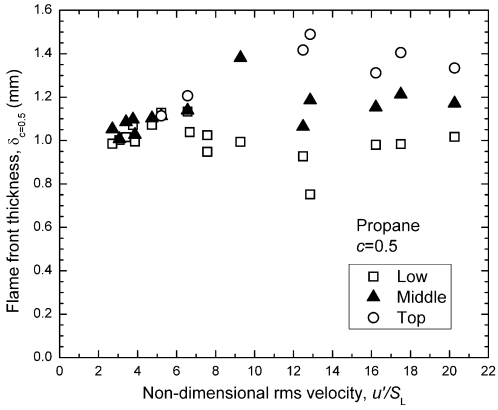

Fig. 5. Flame front thickness at $c = 0.5$ for propane flames as a function of non-dimensional turbulence rms velocity at different sections of the flame.

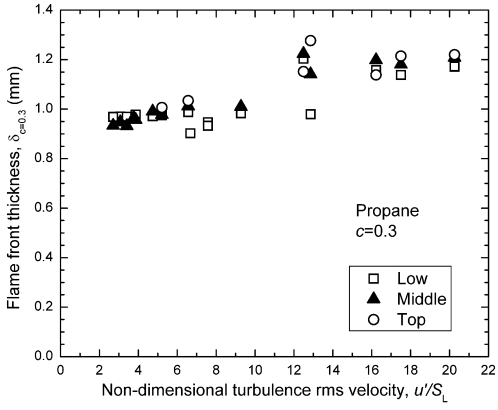

Fig. 6. Flame front thickness at $c = 0.3$ for propane flames as a function of non-dimensional turbulence rms velocity at different sections of the flame.

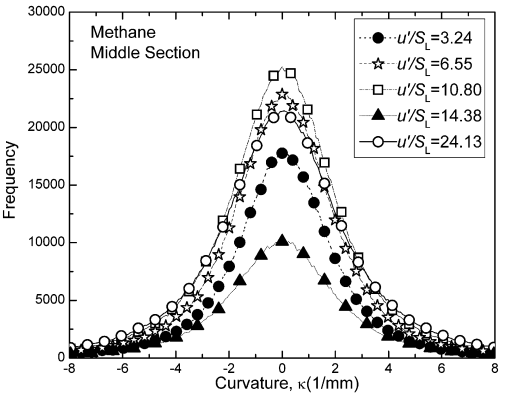

Fig. 7. Probability density functions of curvature for methane flames at various non-dimensional turbulence rms velocities at the middle section of the flame.

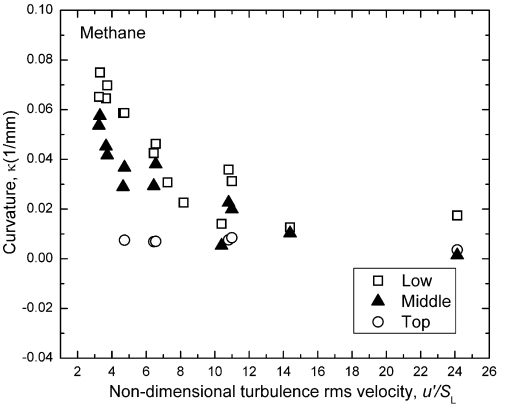

Fig. 8. Mean flame curvature as a function of the non-dimensional turbulence rms velocity for methane flames at different sections of the flame.

[18,23]. Similar curvature pdfs were obtained with propane flames as well as with the lower and top sections of methane flames.

The mean flame curvatures were observed to decline with non-dimensional turbulence intensity in methane flames, Fig. 8. For all three sections of the flame, flame curvatures showed the similar declining trend with u'/S_L. The dependence of flame curvature on u'/S_L was observed to be more modest in propane flames, Fig. 9. Using the measured curvature statistics the term $D\kappa$ in the modified G-equation, proposed for the thin reaction zone regime, has been evaluated for methane and propane flames studied in this work. The results of this exercise are shown in Figs. 10 and 11, for methane and propane flames, respectively. Note that $D\kappa$ data are presented for conditions where the non-dimensional turbulence rms velocity is larger than about 8. The magnitude of the

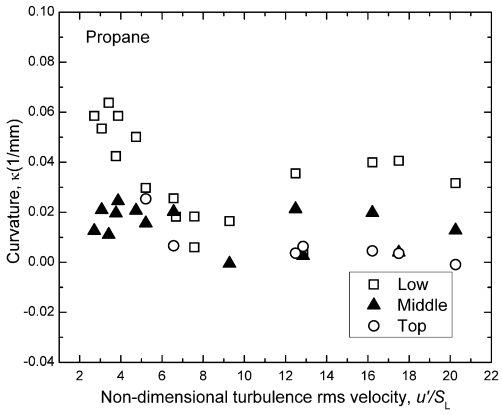

Fig. 9. Mean flame curvature as a function of the non-dimensional turbulence rms velocity for propane flames at different sections of the flame.

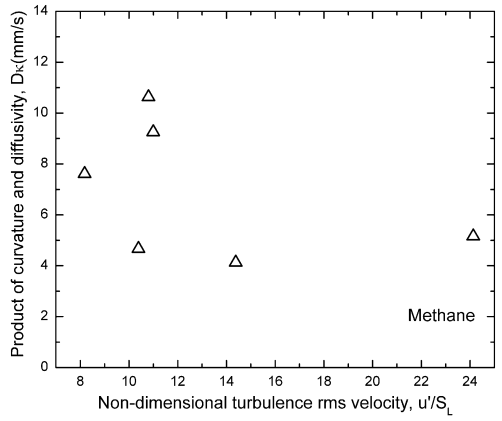

Fig. 10. Product of molecular diffusivity and flame curvature as a function of non-dimensional turbulence rms velocity for methane flames.

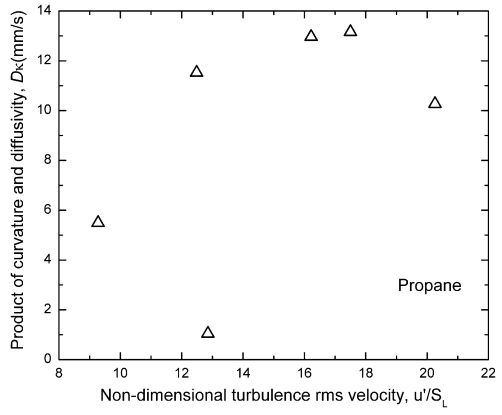

Fig. 11. Product of molecular diffusivity and flame curvature as a function of non-dimensional turbulence rms velocity for propane flames.

term $D\kappa$ is much smaller than the laminar burning velocity for both methane and propane flames, Figs. 10 and 11.

It is proposed that the magnitude of $D\kappa$ would be much greater than the laminar burning velocity so that the modified G-equation, Eq. (1), would be able to represent premixed turbulent combustion in the thin reaction zone regime [4]. However, results presented in Figs. 10 and 11 do not support this proposition. The basis of the level set equations for premixed turbulent combustion has its origin in the assumption of thin flame structures with a passive surface character. Equation (1) is an extension of the level set equation, derived for corrugated flame region, to thin reaction zones regime. Current findings and the experimental evidence reported previously, e.g., [5–8], suggest that the validity range of thin flame assumption with a passive surface should not be extended to higher turbulence intensities and Karlovitz numbers, and the significant deviations in the scalar structure of the flame front from that of a laminar flamelet should be taken into consideration.

The derivation of Eq. (1) [4] relies on the numerical data from 2D direct simulations of premixed turbulent combustion reported in [3]. Then, for purely mechanistic purposes, 2D measurements reported here for comparison purposes should be appropriate. However, as explicitly stated in the experimental section, 2D measurements may not capture all aspects of the 3D structure. But, as demonstrated in [21], the differences are not significant enough to change the main conclusion of this work. Further, it was shown in [24], by separate 2D and 3D Rayleigh scattering measurements on methane–air flames, 2D and 3D flame thickness results displayed almost the same behaviour with turbulence intensity. 2D results were systematically higher, about 10–20%, than 3D results at turbulence intensities of $u'/S_L \sim 5$ to about 19.

4. Concluding remarks

Premixed turbulent flames of methane–air and propane–air stabilized on a bunsen type burner were studied in order to understand the structure of the flame front in the thin reaction zone regime. The flame front data were obtained using planar Rayleigh scattering, and particle image velocimetry was used to measure instantaneous velocity field for the experimental conditions studied. The fuel–air equivalence ratio range was from lean 0.6 to stoichiometric for methane flames, and from 0.7 to stoichiometric for propane flames. The non-dimensional turbulent rms velocity, u'/S_L, covered a range from 3 to 24.

Flame front thickness increased slightly with increasing non-dimensional turbulence rms velocity in both methane and propane flames, although the flame thickening was more prominent in

propane flames. There was not any significant difference in flame thickening whether the flame thickness is evaluated at progress variable 0.5 or 0.3.

The probability density function of curvature showed a Gaussian-like distribution at all turbulence intensities in both methane and propane flames, at all sections of the flame.

The value of the term $D\kappa$, the product of molecular diffusivity evaluated at reaction zone conditions and the flame front curvature, has been shown to be smaller than the magnitude of the laminar burning velocity. This finding questions the validity of extending the level set formulation, developed for corrugated flames region, into the thin reaction zone regime by modifying the local flame propagation by the term $D\kappa$ in addition to laminar burning velocity.

Acknowledgments

The work reported in this paper was supported by a Collaborative Research Opportunities (NSERC-CRO) grant from Natural Sciences and Engineering Research Council of Canada. The authors thank Prof. N. Ashgriz for the loan of the PIV-system and Dr. D. Pavé for the help with setting up the Rayleigh measurement system.

References

[1] D. Bradley, P.H. Gaskell, X.J. Gu, *Combust. Flame* 96 (1994) 221–248.
[2] N. Peters, *J. Fluid Mech.* 384 (1999) 107–132.
[3] N. Peters, P. Terhoeven, J.H. Chen, T. Echekki, *Proc. Combust. Inst.* 27 (1998) 833–839.
[4] N. Peters, *Turbulent Combustion*, Cambridge University Press, Cambridge, UK, 2000, p. 106.
[5] Y.-C. Chen, R.W. Bilger, *Combust. Flame* 131 (2002) 400–435.
[6] Ö.L. Gülder, G.J. Smallwood, R. Wong, et al., *Combust. Flame* 120 (2000) 407–416.
[7] Ö.L. Gülder, G.J. Smallwood, *Combust. Sci. Technol.* 179 (2007) 191–206.
[8] Ö.L. Gülder, *Proc. Combust. Inst.* 31 (2007) 1369–1375.
[9] A.C. Eckbreth, *Laser Diagnostics for Combustion Temperature and Diagnostics*, second ed., Gordon and Breach Publishers, Kent, UK, 1996.
[10] R.W. Dibble, R.E. Hollenbach, *Proc. Combust. Inst.* 18 (1981) 1489–1499.
[11] R.B. Miles, W.R. Lempert, J.N. Forkey, *Meas. Sci. Technol.* 12 (2001) R33–R51.
[12] F. Dinkelacker, A. Soika, D. Most, et al., *Proc. Combust. Inst.* 27 (1998) 857–865.
[13] A. Soika, F. Dinkelacker, A. Leipertz, *Proc. Combust. Inst.* 27 (1998) 785–792.
[14] D.A. Knaus, S.S. Sattler, F.C. Gouldin, *Combust. Flame* 141 (2005) 253–270.
[15] J.A. Sutton, J.F. Driscoll, *Opt. Lett.* 29 (2004) 2620–2622.
[16] H.K. Moffat, D. Goodwin. Available from: <http://www.cantera.org/>.
[17] G.H. Wang, N.T. Clemens, *Exp. Fluids* 37 (2004) 194–205.
[18] M.Z. Haq, C.G.W. Sheppard, R. Wooley, D.A. Greenhalgh, R.D. Lockett, *Combust. Flame* 131 (2002) 1–15.
[19] Y.-C. Chen, *Combust. Theory Model.* 11 (2007) 333–349.
[20] F. Halter, C. Chauveau, N. Djedaili-Chaumeix, I. Gökalp, *Proc. Combust. Inst.* 30 (2005) 201–208.
[21] Y.-C. Chen, M. Kim, J. Han, S. Yun, Y. Yoon, *Proc. Combust. Inst.* 31 (2007) 1327–1335.
[22] S.H. Kim, K. Pitsch, *Phys. Fluids* 19 (2007) 115104–115114.
[23] I.G. Shepherd, R.K. Cheng, T. Plessing, C. Kortschik, N. Peters, *Proc. Combust. Inst.* 29 (2002) 1833–1840.
[24] L.P.H. de Goey, T. Plessing, R.T.E. Hermanns, N. Peters, *Proc. Combust. Inst.* 30 (2005) 859–866.